Charge-carrier transmission across twins in graphene

IOP Publishing Journal of Physics: Condensed Matter
J. Phys.: Condens. Matter **32** (2020) 425003 (9pp) https://doi.org/10.1088/1361-648X/aba0d9

Charge-carrier transmission across twins in graphene

F Arca[1], J P Mendez[2], M Ortiz[2] and M P Ariza[1]

[1] Escuela Técnica Superior de Ingeniería, University of Seville, 41092 Seville, Spain
[2] Division of Engineering and Applied Science, California Institute of Technology, CA, 91125, Pasadena, United States of America

E-mail: mpariza@us.es

Received 12 May 2020, revised 6 June 2020
Accepted for publication 29 June 2020
Published 27 July 2020

Abstract

Twinning is a known accommodation mechanism of graphene that results in low-energy microstructures or twins. In view of their mechanical stability, twins suggest themselves as a possible means of introducing extended defects in graphene leading to the opening of transmission band gaps. We investigate charge-carrier transmission across the twin structures in graphene using the Landauer–Büttiker (LB) formalism in combination with a tight-binding model. We verify the approach by means of selected comparisons with density functional theory (DFT) and non-equilibrium Green's function (NEGF) calculations using the code SIESTA and TRANSIESTA. The calculations reveal that graphene twins open transport gaps depending on the twin geometry up to maximum of 1.15 eV. As previously reported for grain boundaries, we find that localized states arise at dislocation cores in the twin boundaries that introduce peaks near the Fermi level.

Keywords: graphene, twining, charge-carrier transport, Landauer–Büttiker formalism, tight-binding model

(Some figures may appear in colour only in the online journal)

1. Introduction

Owing to its electronic [1] and mechanical properties [2, 3], graphene is under consideration as a next generation material for the nanotransistors industry [4, 5]. However, the absence of a band gap in pristine graphene [6] prevents its use as a semiconductor. Numerous avenues have been pursued with a view to opening transport gaps in graphene. For instance, small band gaps of up to ∼0.4 eV can be induced by applying strain [7, 8]. Gaps in the same range have also been achieved in twisted bilayer graphene devices [9] and in van der Waals heterostructures consisting of a single graphene layer coupled to a hexagonal boron nitride substrate [10]. The introduction of doping elements can result in slightly higher transport gaps of up to 0.67 eV [11]. These band gaps are small compared to that of silicon, 1.12 eV [12], and are not enough for most applications [13]. Isolated defects such as Stone–Wales [14] or vacancies [15] generally fail to open a band gap for the lattice since they only perturb the electronic structure locally. By contrast, extended defects such as certain grain boundaries can induce band gaps as large as 1.54 eV [5, 16, 17].

Twinning is a known deformation mode of graphene [18–20]. Twinning is a piecewise constant deformation of a lattice in which the interface, or 'twin boundary', is undeformed, coherent and such that: (i) the lattices on both sides of the interface are in a stress-free ground state; (ii) the lattice on one side of the interface can be obtained by a lattice-invariant simple shear of the lattice on the other side; and (iii) the lattice on one side of the interface can also be obtained by a rotation of the lattice on the other side. Since, away from the interface, the lattice is in a ground state and the interface is undeformed and coherent, twins are low-energy configurations of the crystal. In addition, since the average deformation following twinning may differ from the identity, twinning provides an accommodation mechanism. Graphene twins have been investigated computationally [21, 22] by introducing twin boundaries in the graphene lattice *ab initio*. Arca *et al* [23] have presented numerical evidence that twinning in fact operates as an accom-

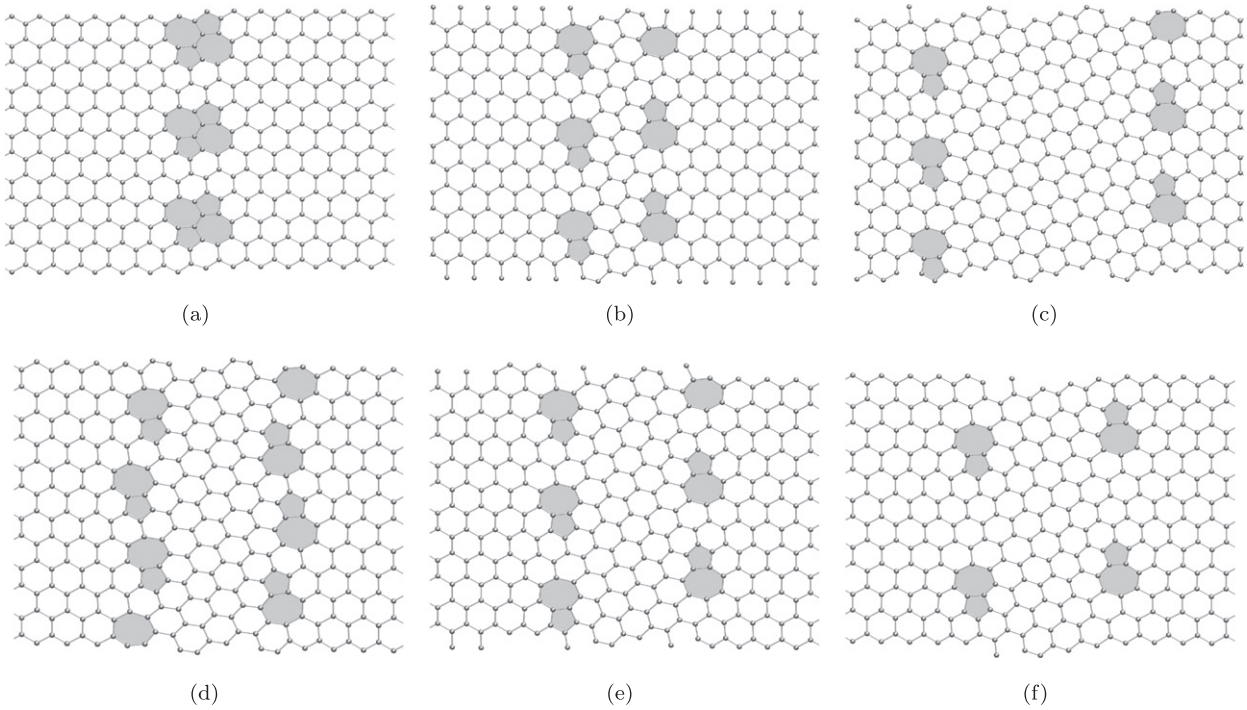

Figure 1. Relaxed atomic configurations of representative dislocations structures and corresponding misorientation angles θ. (a) Stone–Wales array (3, 8); (b) dislocation structures (7, 8), $\theta = 14.4°$; (c) dislocation structures (19, 8), $\theta = 16.1°$; (d) dislocation structures (11, 6), $\theta = 20.3°$; (e) dislocation structures (11, 8), $\theta = 16.1°$; and (f) dislocation structures (11, 12), $\theta = 10.9°$.

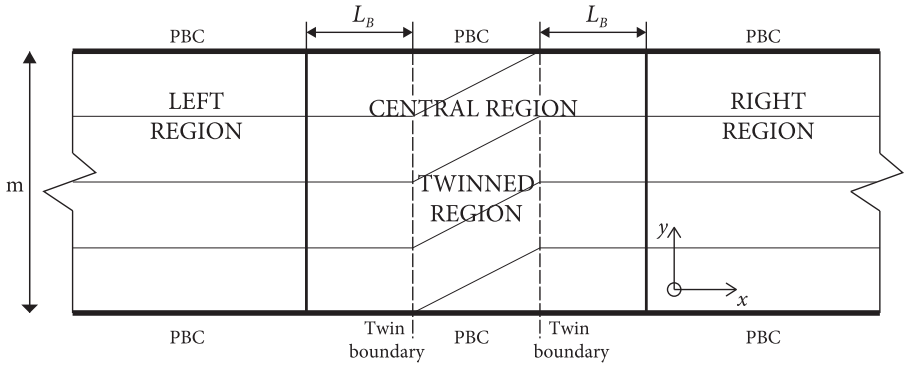

Figure 2. Geometry of the model used to compute the charge-carrier transmission across twins.

modation and relaxation mechanism in graphene, i.e., twins may arise spontaneously in graphene layers containing arrays of dislocations and results in a significant reduction in energy.

In view of their mechanical stability, twins suggest themselves as a possible means of introducing extended defects in graphene leading to the opening of transmission band gaps. Indeed, previous work on charge-carrier transmission in graphene suggest that transport gaps are induced by asymmetric deformations [7, 8]. In the present work, we investigate charge-carrier transmission across the twin structures in graphene using the Landauer–Büttiker (LB) formalism [24–26] in combination with a tight-binding model [27]. These methods have been combined in multiple works before [5, 16, 22, 28, 29]. We verify the approach through selected comparisons with density functional theory (DFT) and non-equilibrium Green's function (NEGF) calculations using the codes SIESTA and TRANSIESTA [30, 31]. The calculations reveal that graphene twins open transport gaps depending on the twin geometry up to maximum of 1.15 eV. This value is consistent with band gaps of up to 1.2 eV reported by Rojas *et al* [22]. As previously reported for grain boundaries [32], we find that localized states arise at dislocation cores in the twin boundaries that introduce peaks near the Fermi level.

2. Periodic dislocation structures in graphene

In this work, we specifically focus on twinned microstructures resulting from the introduction of periodic arrays of parallel dipoles in a single graphene layer, figure 1. The energetics of these structures has been studied in [23] using the computational method presented in [33]. The method consists

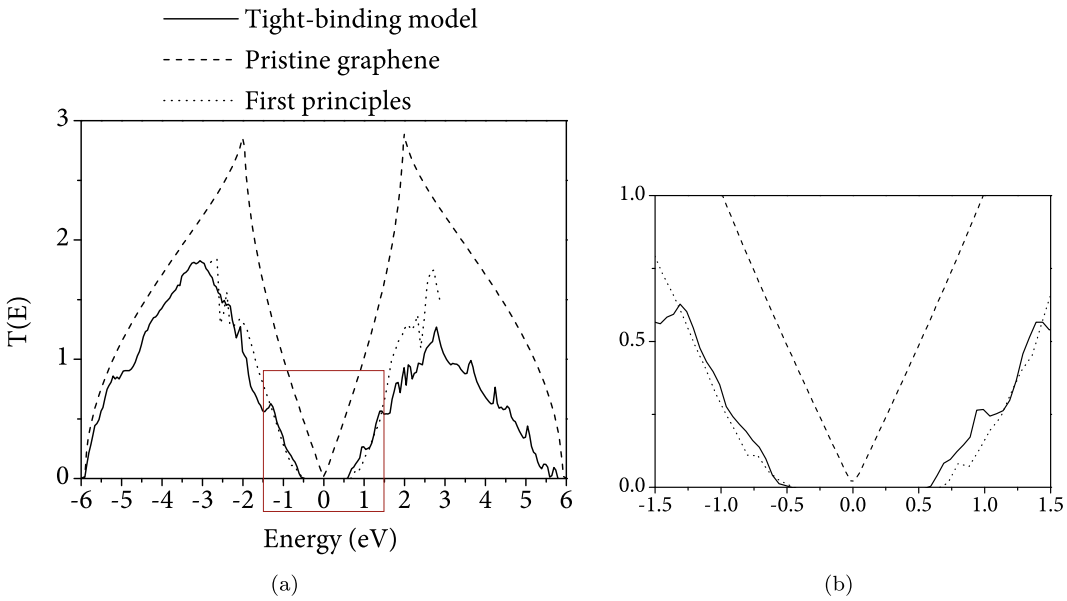

Figure 3. (a) Charge-carrier transmission coefficient per period across the dislocation structures (11, 6) calculated with the tight-binding model and by first principles; (b) detail of the transmission coefficient around zero energy. The Fermi level is set as zero.

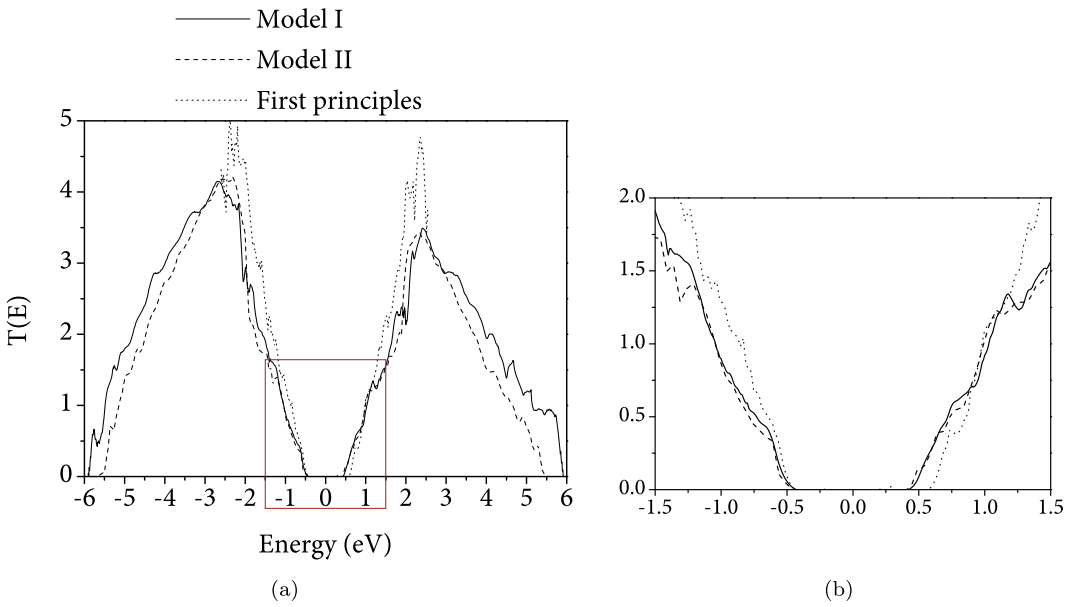

Figure 4. (a) Comparison of charge-carrier transmission coefficient per period across the dislocation structures (15, 12) when investigating flat (model I) or fully relaxed (model II) supercells, by using the tight-binding model and by first principles; (b) detail of the transmission coefficient around zero energy. The Fermi level is chosen as zero.

of a first harmonic step designed to set the desired defect structure into the lattice followed by a fully nonlinear relaxation. In the harmonic step, we employ a force-constant model based on the LCBOPII interatomic potential [34] in order to introduce discrete dislocation dipoles [35, 36] in an otherwise perfect graphene lattice. The defective harmonic configurations are then used as initial conditions for LAMMPS [37] calculations using the full LCBOP potential [38], thus obtaining fully-relaxed configurations. At the end of the relaxation, the lattice between the dislocation arrays is rotated with respect to the parent lattice and the overall microstructure obeys closely the classical twinning relations that identify it as a true twin [23].

Following the notation of [23], the dislocation structures under consideration are parameterized by means of the pair (n, m), where n is the number of zig-zag bonds in the twin, which also measures the width of the twinned region, and m is the number of arm-chair bonds between dipoles, a measure of dipole-plane separation. Figure 1 shows several representative dislocation structures. Except for the shortest dipole, figure 1(a), all equilibrium configurations consist a lamellar twinned region spanning two twin boundaries consisting of

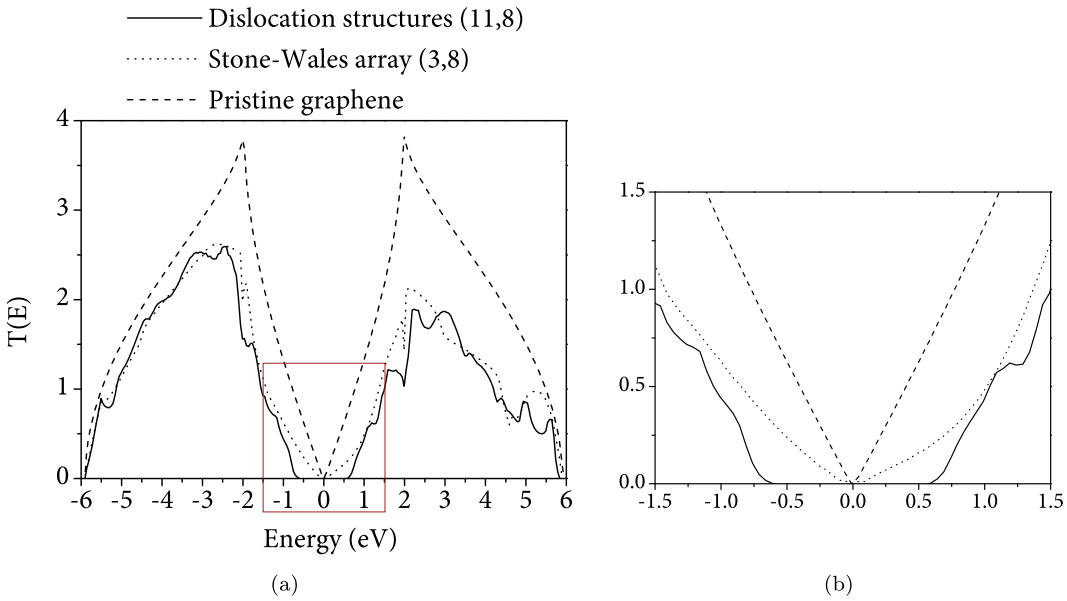

Figure 5. (a) Charge-carrier transmission coefficient per $m = 8$ period across the dislocation structures (3, 8) and (11, 8); (b) detail of the transmission coefficient around zero energy. The Fermi level is set as zero.

arrays of 5–7 dislocations. The misorientation angles between the twinned region and the outside regions, as well as the formation energy of each configuration, depend sensitively on the pair (n, m). These relations can be found in [23], where additional computational details and twinning configurations are reported.

3. Model and methodology

3.1. Model

The computational cell employed for charge-carrier transmission calculations is shown in figure 2. The model is periodic in the y-direction, and it is composed of a central, left and right regions. The central region contains a twin set in through the energy relaxation calculations described in the foregoing. The left and right regions contain defect-free graphene lattices of semi-infinite extent in the x-direction. The distance between the twin boundaries and the interfaces of the regions, L_B, is larger than 75 Å in order for the transition through the regions to be smooth. Since the charge-carrier transmission coefficient is proportional to the number of periods, the y-dimension of the computational may be conveniently restricted to one period of size m.

3.2. Computational methods

In order to compute transport properties, we resort to the Landauer–Büttiker (LB) formalism [25, 26] based on a tight-binding (TB) model [27] as implemented in [17]. The LB formalism provides a theoretical framework for the description of coherent electronic transport with elastic scattering by relating the conductance of a device to its transmission probability. The conductance can be written in terms of the Green's function, which describes the relationship between electronic states for each energy level E of each atom i.

Following [25, 26], the transmission function through the central region at energy level E is

$$T(E) = \mathrm{Tr}\left[\boldsymbol{\Gamma}_{\mathrm{L}}(E)\boldsymbol{G}_{\mathrm{C}}^{\dagger}(E)\boldsymbol{\Gamma}_{\mathrm{R}}(E)\boldsymbol{G}_{\mathrm{C}}(E)\right], \tag{1}$$

where $\boldsymbol{G}_{\mathrm{C}}$ is the Green's function of the central region and $\boldsymbol{\Gamma}_{\mathrm{L}}$ and $\boldsymbol{\Gamma}_{\mathrm{R}}$ account for the coupling between the central region and the left and right regions, respectively. Both functions $\boldsymbol{G}$ and $\boldsymbol{\Gamma}$ are calculated directly from the Hamiltonian of the system for the TB model [27], which accounts for lattice strains [39] by scaling the TB hopping integrals as in [40]. The periodicity in the y-direction is enforced by solving equation (1) in reciprocal $\boldsymbol{k}$-space [41]. In addition, the charge-carrier transmission can be investigated by recourse to the local density of states (LDOS), which represents the number of available states at an atom at an energy level. By the definition of the Green's function, the LDOS of an atom i is

$$\mathrm{LDOS}(E) = -\frac{1}{\pi}\ \mathrm{Im}\left[(\boldsymbol{G}_{\mathrm{C}}^{\dagger})_{ii}\right]. \tag{2}$$

All calculations are carried out under conditions of static equilibrium. In the TB–LB calculations we assume that only the electrons located in the p_z orbitals account for the electronic transport properties [17]. Indeed, these orbitals are normal to the lattice plane and form weak π-bonds with neighboring C atoms. These interactions keep the electrons weakly bounded to the nuclei, unlike the remaining three valence electrons that form strong σ-bonds in the lattice plane. We evaluate equation (1) in the Brillouin zone of the lattice. We verify that convergence is ostensibly attained using 144 $\boldsymbol{k}$-points.

In addition, we simplify the calculations by using flat 2D simulation supercells with constrained out-of-plane displacements. Indeed, previous work on charge-carrier transmission in graphene suggests that the transmission coefficient is nearly

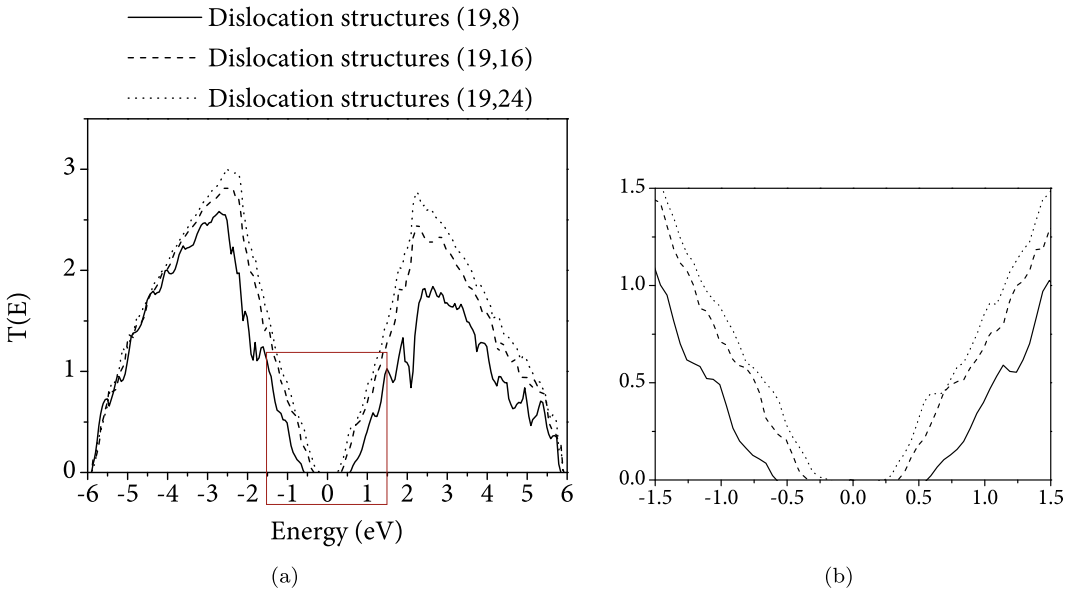

Figure 6. (a) Comparison of charge-carrier transmission coefficient per $m = 8$ period of the dislocation structures (19, 8), (19, 16) and (19, 24); (b) detail of the transmission coefficient around zero energy. The Fermi level is set as zero.

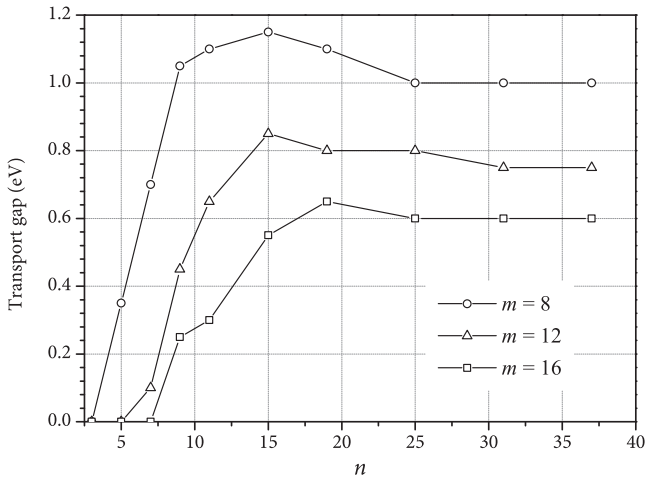

Figure 7. Dependence of the transport gap on the width n of the dipoles for three different dipole separations, $m = 8$, 12, 16.

Table 1. Transmission gap and misorientation angle (θ) of configurations with dipole separations $m = 8$, 12 and 16.

	$m = 8$		$m = 12$		$m = 16$	
	Gap (eV)	θ (°)	Gap (eV)	θ (°)	Gap (eV)	θ (°)
$n = 3$	0.00	0.0	0.00	0.0	0.00	0.0
$n = 5$	0.35	13.3	0.00	8.5	0.00	8.8
$n = 7$	0.70	14.4	0.10	9.4	0.00	9.0
$n = 9$	1.05	16.2	0.45	11.0	0.25	8.5
$n = 11$	1.10	16.1	0.65	10.9	0.30	8.3
$n = 15$	1.15	16.1	0.85	11.1	0.55	8.2
$n = 19$	1.10	16.1	0.80	11.1	0.65	8.2
$n = 25$	1.00	16.1	0.80	11.1	0.60	8.2
$n = 31$	1.00	16.1	0.75	11.1	0.60	8.2
$n = 37$	1.00	16.1	0.75	11.1	0.60	8.2

Table 2. Characteristic values of mismatch and transport gap of dislocation structures with large n.

M	(u_s, v_s)	(u_t, v_t)	d_s (Å)	d_t (Å)	$(d_t - d_s)/d_s$ (%)	Gap (eV)
8	(2, 2)	(3, 1)	8.52	8.87	4.11	1.00
12	(3, 3)	(4, 2)	12.78	13.01	1.80	0.75
16	(4, 4)	(5, 3)	17.04	17.22	1.06	0.60
20	(5, 5)	(6, 4)	21.30	21.44	0.66	0.45
24	(6, 6)	(7, 5)	25.56	25.68	0.47	0.35

identical in fully-relaxed 3D configurations and flat 2D configurations [17].

3.3. Method verification

In order to verify the transmission analysis, we have additionally performed matching first-principles calculations using the DFT-NEGF SIESTA and TRANSIESTA codes [30, 31]. In the calculations, we employ the PBE exchange–correlation functional [42] within the generalized gradient approximation (GGA) and a pseudo-atomic orbitals basis set, the single-ζ basis [43]. Core electrons are approximated by means of smooth norm-conserving pseudopotentials [44]. The DFT calculations are carried out with a mesh cut-off of 400 Ry and a $40 \times 30\,k$-point mesh. A comparison of TB–LB and DFT-NEGF results is shown in figure 3. Both sets of results are in good agreement, particularly near the Fermi level, where equilibrium calculations are most accurate.

We verify the accuracy of the flat-cell 2D approximation, with constrained out-of-plane displacements, for the case of twinned graphene in the (15, 12) configuration, figure 4. As may be seen from the figure, the moderate out-of-plane warping of the lattice in the fully-relaxed configuration (model II) does not significantly modify the charge carrier transmission

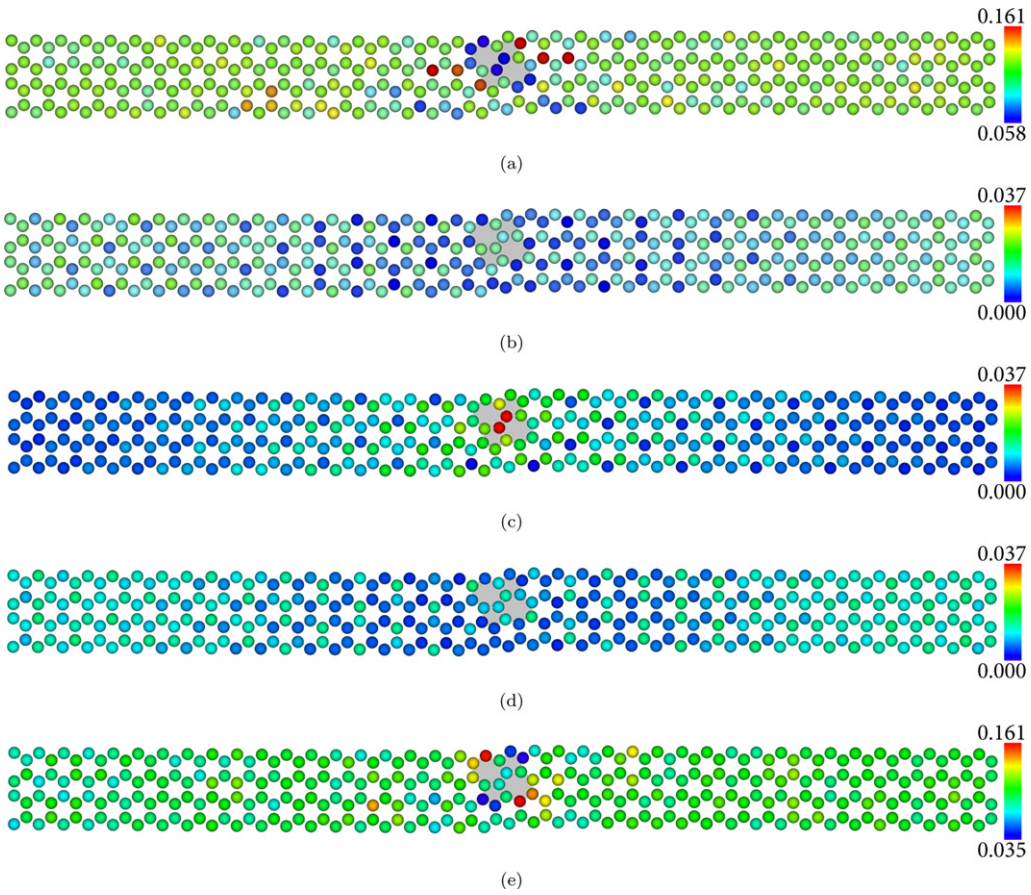

Figure 8. Local density of states of the Stone–Wales array (3, 8) at (a) $E = -1.55$ eV; (b) $E = -0.25$ eV; (c) $E = 0.05$ eV; (d) $E = 0.25$ eV; and (e) $E = 1.55$ eV. The Fermi level is set as zero.

curves. The results from both models show ostensibly similar structure and display a nearly identical transport gap of 0.85 eV, with bears out the 2D approximation.

4. Transmission across dislocation structures

We have investigated charge-carrier transmission across the graphene twin structures using the computational methods just described. Figure 5 shows the charge-carrier transmission across two representative dislocation structures, (3, 8) and (11, 8). As may be seen from the figure, both configurations reduce the conductivity of pristine graphene and break the electron–hole symmetry. This effect is expected given that the transmission of holes is higher than that of electrons, as observed in graphene containing topological defects, e.g., Stone–Wales [14] or grain boundaries [17, 32]. Remarkably, only the twinning configuration (11, 8) displays a transport gap (figure 1).

The width of the transport gaps opened by twinning depends on the dislocation density, as observed in figure 6. Specifically, the higher the dislocation separation, m, the smaller the transport gap. Furthermore, the transport gap also depends on the width n of the twinned region for configurations with small and medium values of n. This effect is shown in figure 7 for the cases $m = 8$, 12 and 16. It is observed that the transport gap increases up to a maximum at approximately $n = 15$ and subsequently decreases slightly to a constant value solely dependent on m beyond $n \sim 25$. This asymptotic value for large n may be regarded as a characteristic transport gap for a given m. Coincidentally, analyses of isolated dislocation dipoles in graphene reveal that the dislocation cores cease to interact at approximately that twin width [33, 45]. The opening of band gaps may be traced to localized wave functions that arise at—and bind to—dislocation cores. This localized wave functions decay quickly away from the dislocation cores with the result that, beyond a certain dipole separation, they cease to overlap significantly. In that range, the magnitude of the bandgap saturates and become independent of the separation between the interfaces.

In table 1 we collect the gap sizes exhibited by a range of dislocation structures. Most twinning structures, $n \geqslant 5$, open a transport gap, with a maximum of 1.15 eV for the (15, 8) configuration. This transport gap therefore suggests itself as an upper limit for twinned graphene, comparable to similar values for asymmetric grain boundaries [16, 17]. As already noted, the misorientation angle also differs between microstructures. However, misorientation and gap size do not appear to be directly correlated. Indeed, configurations with small n entail significant misorientation but no transport gap, especially for large m. Previous articles on charge-carrier transmission in graphene suggest that transport gaps are induced by asymmetric deformations [7, 8]. In view of these considerations, we

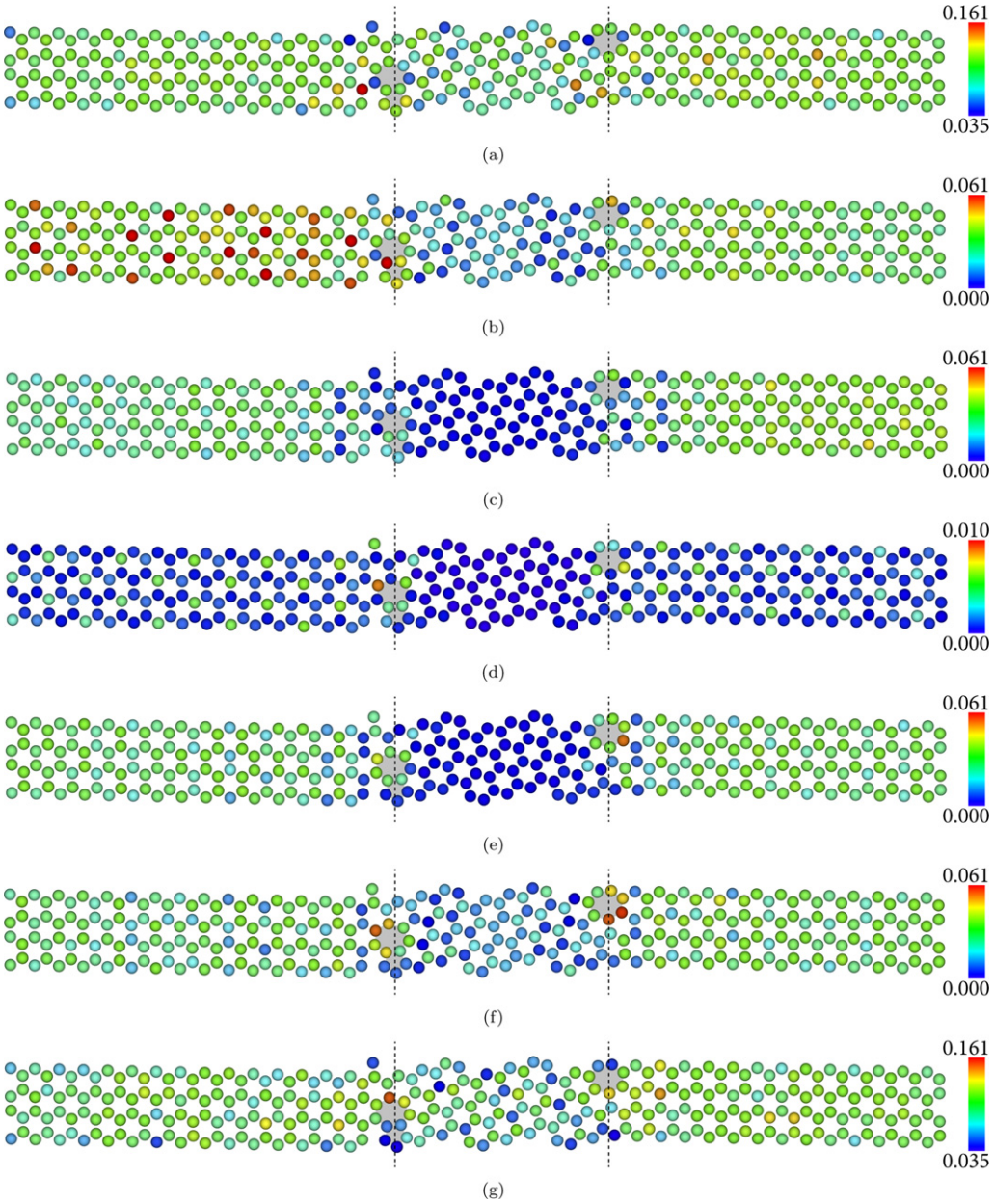

Figure 9. Local density of states of the dislocation structures (19, 8) at (a) $E = -1.55$ eV; (b) $E = -0.60$ eV; (c) $E = -0.55$ eV; (d) $E = 0.00$ eV; (e) $E = 0.55$ eV; (f) $E = 0.60$ eV; and (g) $E = 1.55$ eV. The Fermi level is set as zero.

seek to peg the transmission properties to the lattice mismatch measure [16],

$$\frac{\Delta d}{d} = \frac{d_t - d_s}{d_s}, \tag{3}$$

where d_s and d_t are the periodic y-sizes of the side regions and the twinned region, respectively, in their undeformed configurations. We specifically calculate d as [16]

$$d_t = \sqrt{3}a\sqrt{u_t^2 + u_t v_t + v_t^2} \tag{4}$$

where $a = 1.42$ Å is the graphene lattice constant for the LCBOP potential and (u_t, v_t) is the translation vector of the twinned region along the y-direction in terms of Bravais lattice coordinates. The value of d_s follows analogously for the side regions.

Table 2 collects the values of the transport gaps for large twin width and the corresponding lattice mismatch. As may be seen from the table, configurations with a small dipole separation present a high mismatch, i.e., a large strain along the twin boundaries, and simultaneously a wide transport gap. This correlation is in agreement with previous work [7, 8]. In table 2 we also observe that configurations with high m have high values of (u_t, v_t). This correlation suggests that twin configurations with larger dipole separation require larger dipole widths to open a transport gap.

Finally, we analyze the local density of state (LDOS) with a view to deriving additional insight into the fine electronic structure. Figures 8 and 9, show the LDOS computed for the (3, 8) and (19, 8) configurations, respectively, at different energy levels in the vicinity of the Fermi level. We recall that the

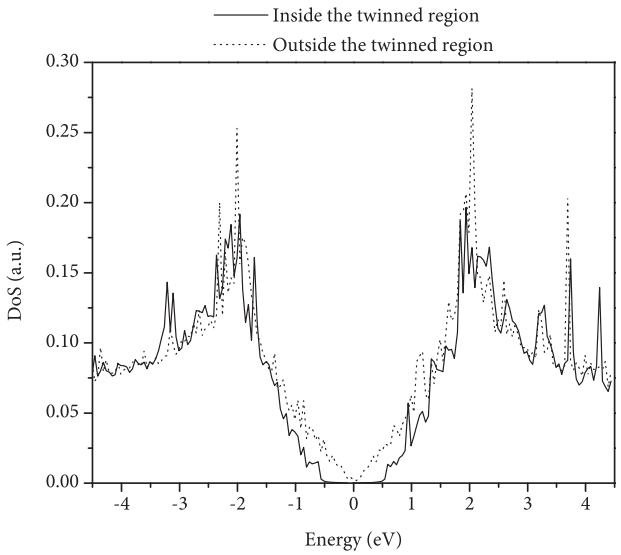

Figure 10. DOS inside and outside the twinned region for the (19, 8) configuration.

(3, 8) configuration consists of Stone–Wales arrays with no discernible twinned region, figure 1. For this configuration, the LDOS is perturbed by localized states at the Stone–Wales defect cores corresponding to peaks near the Fermi energy. These localized states decrease the electronic transmission across these defects and cause a reduction in overall conductivity. This reduction is in accordance with previous tight-binding studies of the electronic properties of Stones–Wales defects in graphene [46], which show that 7–5 Stone–Wales defects alter the local electronic structure and reduce the overall conductivity but do not suffice to open a band gap in general. By contrast, the (19, 8) configuration consists of 5–7 dislocations separated by a twinned region. Under such conditions, the LDOS of the twin vanishes in the energy range of −0.55 eV to 0.55 eV. By contrast, the zero band gap property of pristine graphene is preserved elsewhere in the lattice, figure 10. As previously reported for grain boundaries [32], localized states arise at dislocation cores and introduce peaks near the Fermi level, figures 8 and 9.

5. Conclusion

Owing its mechanical stability and role as low-energy deformation mechanism, twinning suggests itself as an effective means of introducing extended defects in graphene leading to the opening of transmission band gaps. We have investigated the charge-carrier transmission across twin structures in graphene using the Landauer–Büttiker (LB) formalism in combination with a tight-binding model. We have verified our approach by means of selected comparisons with density functional theory (DFT) and non-equilibrium Green's function (NEGF) calculations using the SIESTA and TRANSIESTA codes. Our calculations reveal that graphene twins open transport gaps depending on the twin geometry up to maximum of 1.15 eV. As previously reported for grain boundaries, we have found that localized states arise at dislocation cores in the twin boundaries that introduce peaks near the Fermi level.

Acknowledgments

This research has been funded by the Consejería de Economía, Innovación, Ciencia y Empleo of Junta de Andalucía under Grant Number P12-TEP-850 and the Ministerio de Ciencia, Innovación y Universidades of Spain under Grant Number RTI2018-094325-B-I00.

ORCID iDs

F Arca https://orcid.org/0000-0003-2473-4589
J P Mendez https://orcid.org/0000-0002-9493-0879
M P Ariza https://orcid.org/0000-0003-0266-0216

References

[1] Geim A K and Novoselov K S 2007 The rise of graphene *Nat. Mater.* **6** 183–91
[2] Lee C, Wei X, Kysar J W and Hone J 2008 Measurement of the elastic properties and intrinsic strength of monolayer graphene *Science* **321** 385–8
[3] Zhang T, Li X and Gao H 2014 Defects controlled wrinkling and topological design in graphene *J. Mech. Phys. Solids* **67** 2–13
[4] Bae S *et al* 2010 Roll-to-roll production of 30-inch graphene films for transparent electrodes *Nat. Nanotechnol.* **5** 574–8
[5] Zhang J, Gao J, Liu L and Zhao J 2012 Electronic and transport gaps of graphene opened by grain boundaries *J. Appl. Phys.* **112** 053713
[6] Novoselov K S, Geim A K, Morozov S V, Jiang D, Zhang Y, Dubonos S V, Grigorieva I V and Firsov A A 2004 Electric field effect in atomically thin carbon films *Science* **306** 666–9
[7] Ni Z H, Yu T, Lu Y H, Wang Y Y, Feng Y P and Shen Z X 2008 Uniaxial strain on graphene: Raman spectroscopy study and band-gap opening *ACS Nano* **2** 2301–5
[8] Gui G, Li J and Zhong J 2008 Band structure engineering of graphene by strain: first-principles calculations *Phys. Rev.* B **78** 075435
[9] Cao Y *et al* 2018 Correlated insulator behaviour at half-filling in magic angle graphene superlattices *Nature* **556** 4
[10] Hunt B *et al* 2013 Massive Dirac fermions and Hofstadter butterfly in a van der Waals heterostructure *Science* **340** 1427–30
[11] Denis P A 2010 Band gap opening of monolayer and bilayer graphene doped with aluminium, silicon, phosphorus, and sulphur *Chem. Phys. Lett.* **492** 251–7
[12] Shenai K, Scott R S and Baliga B J 1989 Optimum semiconductors for high-power electronics *IEEE Trans. Electron Devices* **36** 1811–23
[13] Tolbert L, Ozpineci B, Islam S and Chinthavali M 2003 Wide bandgap semiconductors for utility applications *Proc. of the IASTED Multi-Conf.-Power and Energy Systems* vol 7 p 1
[14] Mendez J P and Ariza M P 2016 Harmonic model of graphene based on a tight binding interatomic potential *J. Mech. Phys. Solids* **93** 198–223 special issue in honor of Michael Ortiz
[15] Lherbier A, Dubois S M-M, Declerck X, Niquet Y-M, Roche S and Charlier J-C 2012 Transport properties of graphene containing structural defects *Phys. Rev.* B **86** 075402

[16] Yazyev O V and Louie S G 2010 Electronic transport in polycrystalline graphene *Nat. Mater.* **9** 806–9
[17] Mendez J P, Arca F, Ramos J, Ortiz M and Ariza M P 2018 Charge carrier transport across grain boundaries in graphene *Acta Mater.* **154** 199–206
[18] An J *et al* 2011 Domain (grain) boundaries and evidence of twin-like structures in chemically vapor deposited grown graphene *ACS Nano* **5** 2433–9
[19] Rooney A P *et al* 2018 Anomalous twin boundaries in two dimensional materials *Nat. Commun.* **9** 3597
[20] Bhattacharya K 2003 *Microstructure of Martensite: Why it Forms and How it Gives Rise to the Shape-Memory Effect* (Oxford: Oxford University Press)
[21] Terrones H and Mackay A L 1992 The geometry of hypothetical curved graphite structures *Carbon* **30** 1251–60 special issue on fullerness
[22] Rojas D F, Sun D and Ponga M 2019 Twinning in two-dimensional materials and its application to electronic properties *Electron. Struct.* **1** 025001
[23] Arca F, Mendez J P, Ortiz M and Ariza M P 2020 Spontaneous twinning as an accommodation mechanism in monolayer graphene *Eur. J. Mech.* A **80** 103923
[24] Foa Torres L, Roche S and Charlier J 2014 *Introduction to Graphene-Based Nanomaterials: From Electronic Structure to Quantum Transport* (Cambridge: Cambridge University Press)
[25] Datta S 1995 Cambridge studies in semiconductor physics and microelectronic engineering *Electronic Transport in Mesoscopic Systems* (Cambridge: Cambridge University Press)
[26] Datta S 2005 *Atom to Transistor* (Cambridge: Cambridge University Press)
[27] Xu C H, Wang C Z, Chan C T and Ho K M 1992 A transferable tight-binding potential for carbon *J. Phys.: Condens. Matter* **4** 6047–54
[28] Shirodkar S N and Waghmare U V 2012 Electronic and vibrational signatures of stone-wales defects in graphene: first-principles analysis *Phys. Rev.* B **86** 165401
[29] Luican-Mayer A *et al* 2016 Localized electronic states at grain boundaries on the surface of graphene and graphite *2D Mater.* **3** 031005
[30] Soler J M, Artacho E, Gale J D, García A, Junquera J, Ordejón P and Sánchez-Portal D 2002 The SIESTA method for *ab initio* order-*n* materials simulation *J. Phys.: Condens. Matter* **14** 2745–79
[31] Brandbyge M, Mozos J L, Ordejón P, Taylor J and Stokbro K 2002 Density-functional method for nonequilibrium electron transport *Phys. Rev.* B **65** 165401
[32] Zhang H, Lee G, Gong C, Colombo L and Cho K 2014 Grain boundary effect on electrical transport properties of graphene *J. Phys. Chem.* C **118** 2338–43
[33] Arca F, Mendez J P, Ortiz M and Ariza M P 2019 Steric interference in bilayer graphene with point dislocations *Nanomaterials* **9** 1012
[34] Los J H, Ghiringhelli L M, Meijer E J and Fasolino A 2005 Improved long-range reactive bond-order potential for carbon. I. Construction *Phys. Rev.* B **72** 214102
[35] Ariza M P and Ortiz M 2005 Discrete crystal elasticity and discrete dislocations in crystals *Arch. Ration. Mech. Anal.* **178** 149–226
[36] Ariza M P and Ortiz M 2010 Discrete dislocations in graphene *J. Mech. Phys. Solids* **58** 710–34
[37] Plimpton S 1995 Fast parallel algorithms for short-range molecular dynamics *J. Comput. Phys.* **117** 1–19
[38] Los J H and Fasolino A 2003 Intrinsic long-range bond-order potential for carbon: performance in Monte Carlo simulations of graphitization *Phys. Rev.* B **68** 024107
[39] Cadelano E, Palla P L, Giordano S and Colombo L 2009 Nonlinear elasticity of monolayer graphene *Phys. Rev. Lett.* **102** 235502
[40] Goodwin L, Skinner A J and Pettifor D G 1989 Generating transferable tight-binding parameters: application to silicon *Europhys. Lett.* **9** 701–6
[41] Kittel C 2004 *Introduction to Solid State Physics* 8th edn (New York: Wiley)
[42] Perdew J P, Burke K and Ernzerhof M 1996 Generalized gradient approximation made simple *Phys. Rev. Lett.* **77** 3865–8
[43] Junquera J, Paz O, Sańchez-Portal D and Artacho E 2001 Numerical atomic orbitals for linear-scaling calculations *Phys. Rev.* B **64** 235111
[44] Troullier N and Martins J L 1991 Efficient pseudopotentials for plane-wave calculations *Phys. Rev.* B **43** 1993–2006
[45] Chen S and Chrzan D 2011 Continuum theory of dislocations and buckling in graphene *Phys. Rev.* B **84** 12
[46] Méndez J 2015 Harmonic/nonharmonic model of graphene and its structural defects based on a tight binding interatomic potential *PhD Thesis* University of Seville